Enhanced random lasing from distributed Bragg reflector assisted Au-ZnO nanowire Schottky diode

Sunayna B. Bashar, Mohammad Suja, Wenhao Shi, and Jianlin Liu

Citation: Applied Physics Letters **109**, 192101 (2016); doi: 10.1063/1.4967177
View online: http://dx.doi.org/10.1063/1.4967177
View Table of Contents: http://scitation.aip.org/content/aip/journal/apl/109/19?ver=pdfcov
Published by the AIP Publishing

Enhanced random lasing from distributed Bragg reflector assisted Au-ZnO nanowire Schottky diode

Sunayna B. Bashar, Mohammad Suja, Wenhao Shi, and Jianlin Liu[a)]
Department of Electrical and Computer Engineering, University of California, Riverside, California 92521, USA

(Received 6 September 2016; accepted 23 October 2016; published online 7 November 2016)

An electrically pumped ultraviolet random laser based on an Au-ZnO nanowire Schottky junction on top of a SiO_2/SiN_x distributed Bragg reflector (DBR) has been fabricated. Electrical characterization shows typical Schottky diode current-voltage characteristics. Evident random lasing behavior is observed from electroluminescence measurement at room temperature. In comparison with a reference device having similar nanowire morphology but no DBR, this laser demonstrates almost 1.8 times reduction in threshold current and 4 times enhancement in output power. The performance enhancement originates from the incorporation of the DBR structure, which provides high reflectivity in the designed wavelength range. *Published by AIP Publishing.*
[http://dx.doi.org/10.1063/1.4967177]

Extensive research has been done on random lasers due to its operational and structural simplicity with potential applications in the areas of speckle-free imaging, sensing, medical diagnostics, and so on.[1–6] ZnO proves to be a promising candidate for ultraviolet (UV) random lasing because of its wide direct bandgap (3.37 eV), large exciton binding energy (60 meV), large oscillator strength providing high gain, and high refractive index (≈2.5) that favors strong scattering inside ZnO random media, a fundamental requirement for random lasers.[7,8] Earlier effort on ZnO random laser actions was mainly focused on optical pumping of various ZnO polycrystalline films, powders, nanowire networks, and so on.[9–15] Recently, electrically pumped ZnO random lasers have been achieved based on both thin films[16–20] and randomly distributed nanowire arrays.[21–29] Due to an existence of ample air gaps among self-assembled nanowires, light scattering becomes very effective, making randomly distributed nanowire network a desirable optical cavity among others for random laser applications. As a matter of fact, ZnO nanowire based random laser diodes have been realized using p-n homojunctions,[21–23] heterojunctions,[24,25] metal-insulator-semiconductor (MIS) structures,[26–28] and Schottky junctions.[29]

To further advance ZnO-based random lasers toward potential practical applications, improved design is necessary to continue to reduce the threshold current and increase the output power of existing devices. For example, with the inclusion of a distributed Bragg reflector (DBR) structure, a p-ZnO nanowire/n-ZnO thin film junction has achieved a significant enhancement in its lasing performance.[23] Nevertheless, p-type ZnO is often either difficult to achieve or unreliable.[30] In this paper, we report a DBR-assisted Au-ZnO nanowire Schottky junction laser based on undoped n-type nanowires. The designed DBR structure of 10-period alternating 65.07-nm SiO_2 and 47.5-nm SiN_x layers provides high reflectivity at the bottom of the ZnO nanowire laser, thus causing more light to be scattered among the nanowires. As a result, almost 1.8 times reduction in threshold current and 4 times enhancement in output power are achieved.

First, we designed quarter-wavelength DBR with SiO_2 and SiN_x as two dielectric layers using the following equation:

$$n_H l_H = n_L l_L = \lambda/4,$$

where λ is operating wavelength, SiN_x refractive index $n_H = 2$, and thickness is l_H, SiO_2 refractive index $n_L = 1.46$, and thickness is l_L. Substituting the refractive index values in the equation yields SiN_x thickness $l_H = 47.5$ nm, and SiO_2 thickness $l_L = 65.07$ nm. The reflection spectrum was simulated based on Transfer Matrix Method using MATLAB.[17,23] Next, according to the design, a 10-period SiO_2 (65.07 nm)/SiN_x (47.5 nm) DBR structure was deposited on top of an n-type Si (100) substrate by using plasma enhanced chemical vapor deposition (PECVD). Standard procedures with reactant gases NH_3/SiH_4 and N_2O/SiH_4 were used for the process. Plasma power was maintained at 25 W with a source radio frequency (RF) of 13.56 MHz and substrate temperature was kept at 250 °C. After the deposition of DBR, the sample was transferred to a molecular beam epitaxy (MBE) chamber to grow an undoped ZnO thin film. During the MBE growth, a thin MgO/ZnO buffer layer of ∼5 nm/5 nm was first deposited on the substrate for 6 min under a O_2 flow rate of 1.5 sccm, and a Mg and Zn cell temperature of 455 °C and 340 °C, respectively. Substrate temperature was kept at 400 °C for this step. Then a thicker ZnO buffer layer of ∼100 nm was deposited for 40 min with the same Zn cell temperature and O_2 flow rate. Finally, a ZnO layer of ∼800 nm was grown, which acts as seed for subsequent nanowire growth. During this step, a Zn effusion cell temperature of 352 °C and a O_2 flow rate of 1.5 sccm, a substrate temperature of 550 °C, and a growth time of 4 h were used. For the entire growth period, an RF plasma source with a plasma power of 400 W was used to feed the oxygen source into the chamber. The subsequent growth of undoped ZnO nanowires was carried out in a chemical vapor deposition

[a)]Author to whom correspondence should be addressed. Electronic mail: jianlin@ece.ucr.edu

(CVD) furnace. The MBE grown seed layer sample was directly transferred into the CVD and positioned in the center of the furnace. Zinc powder (99.9999% Sigma Aldrich) contained in a silica bottle was used as the source material and placed ~1 cm upstream from the sample. The 300-sccm Ar/O_2 (molar ratio 99.5:0.5) as the reaction gas and 600-sccm N_2 as the carrier gas were kept flowing in the furnace during the growth. Growth temperature and time were 520 °C and 1 h, respectively. During the nanowire growth, part of the sample was covered by a piece of silicon intentionally to exclude the growth of nanowires on the area, where a metal contact will be formed during the device fabrication.

To fabricate the laser devices, first a Ti/Au (10 nm/100 nm) was deposited onto the exposed ZnO thin film area by e-beam evaporation as an Ohmic contact. Then, a thin Au layer of 10 nm was deposited by e-beam evaporation on top of the nanowires to form Schottky junction. Due to the dense distribution of nanowires and limited deposition of Au, Au cannot reach the underlying film. Finally, an ITO glass slide (15–25 Ω/sq) was clamped on top of Au metal for steady electrical connection.

For morphological inspection, a Philips XL 30 Scanning Electron Microscope (SEM) system was used. X-ray diffraction (XRD) patterns were recorded by a Bruker D8 Advance X-ray diffractometer. Current-voltage (I–V) measurements were performed using a semiconductor parameter analyzer (Agilent 4155C) equipped with a probe station (Signatone, model H150). Photoluminescence (PL) spectra were collected by a homebuilt spectrometer system. The system consists of an Oriel monochromator, a photomultiplier detector, a lock-in amplifier, a chopper, a Janis cryostat, and a 325-nm He-Cd laser (Kimmon Koha) as the excitation source. Electroluminescence (EL) measurements were carried out at room temperature using the same setup as PL except that the excitation source was a dc power supply (HP E3630A) and a heat sink was used. Output power from the device was measured by a Thorlabs PM100 power meter. A reference sample having similar morphology of nanowires and no DBR structure was fabricated and characterized as well for comparison under the same experimental conditions.

Figure 1(a) shows the simulated reflection spectrum of the designed 10-period DBR structure around the desired wavelength range. As seen from the spectrum, the reflectivity maximizes at the operating wavelengths near 380 nm, which is the ZnO near band edge emission wavelength. As a matter of fact, the reflection response Γ from the DBR at operating wavelength $\lambda = 380$ nm can be simply expressed as:

$$\Gamma = \frac{1 - \left(\frac{n_H}{n_L}\right)^{2N} \frac{n_H^2}{n_a n_b}}{1 + \left(\frac{n_H}{n_L}\right)^{2N} \frac{n_H^2}{n_a n_b}},$$

where the refractive index of air $n_a = 1$, Si substrate refractive index $n_b = 3.5$, and number of bilayer in the DBR $N = 10$. By substituting these values in the equation, the reflection response $\Gamma = -0.99677$. So the reflectivity (%) of this DBR can be calculated as $|\Gamma|^2 = 99.36\%$. The inset of Figure 1(a) shows a side-view SEM image of the actual DBR structure where dotted lines are drawn to distinguish the alternate layers. It can be seen that the alternate layers have quite uniform thickness and smooth interface.

Figure 1(b) shows a top-view SEM image of the ZnO seed film. Packed columnar structures can be seen, which is

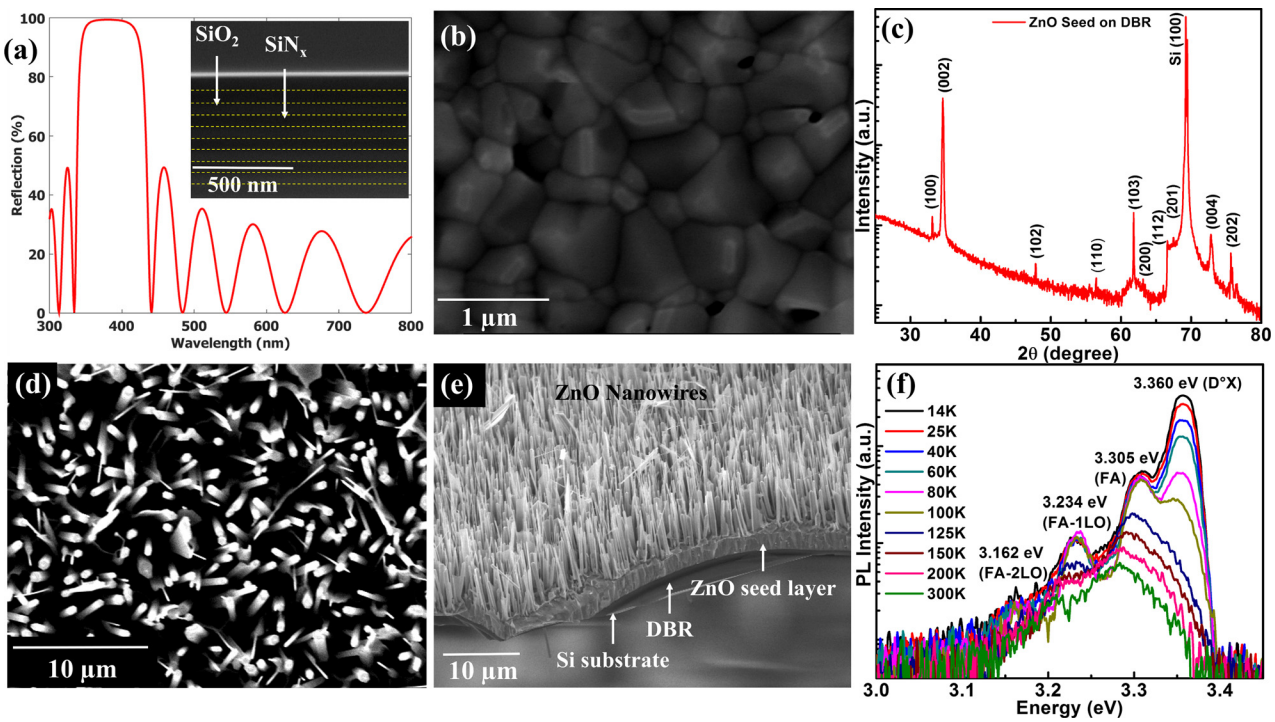

FIG. 1. (a) Simulated reflectance curve of the designed DBR structure that can effectively reflect near band edge emissions of ZnO. Inset shows a side-view SEM image of the DBR structure where the dotted lines represent the interface between alternate layers. (b) SEM image of ZnO seed layer on top of DBR. (c) XRD spectrum of this seed layer. (d) Top-view and (e) side-view SEM images of ZnO nanowires on ZnO seed layer with DBR underneath. (f) Temperature-dependent PL spectra of the ZnO nanowires.

due to the growth of wurtzite ZnO on dielectric DBR. Figure 1(c) shows an XRD spectrum of the ZnO seed layer. Relatively high intensity of ZnO (002) peak with respect to the intensities of other peaks suggests a preferential growth of ZnO along its c-axis. Multi-peak spectrum also confirms multi-grain columnar structure, that is, polycrystalline nature of the seed layer, which is advantageous for the subsequent growth of randomly oriented ZnO nanowires. SEM image and XRD pattern of ZnO seed layer directly grown on Si (reference sample) are shown in Figures S1(a) and S1(b) in the supplementary material, indicating similar morphology as that of the ZnO layer on DBR.

Figures 1(d) and 1(e) show top-view and side-view SEM images of as grown nanowires, respectively. As seen from these SEM images, the nanowires have hexagonal cross-section, indicating that they grow along the c-axis of its wurtzite lattice. Closer investigation of the side-view image reveals that these nanowires are grown on top of hexagonal or pyramidal ZnO island bases with larger lateral sizes. This is because during the early stage of growth, the Zn vapor supersaturation is high, and therefore, the large bases are created; as the growth continues, Zn vapor pressure is reduced, leading to the growth of smaller nanowires.[31] As grown nanowires have an average length of around 7 μm, and are randomly tilted by 10°–15° with respect to the normal to the substrate, the diameters vary in a wide range of approximately 150–550 nm. This kind of morphology creates a random medium to effectively scatter light in the operation of random lasers.[32] In the tilted-view SEM image, individual segments for the nanowires, seed layer, and DBR on top of Si (100) substrate can be identified.

Figure 1(f) shows temperature-dependent PL spectra of as grown ZnO nanowires. The peaks of 3.360 eV and 3.305 eV at 14 K can be assigned as donor bound exciton (D°X) and free electron to acceptor (FA) emissions, respectively.[28,29,33] The D°X emission peak originates from undoped n-type ZnO due to the native donor impurities.[34] The appearance of the FA emission peak suggests the existence of acceptors, which result from unintentional incorporation of nitrogen related complexes.[35] The two peaks red-shift and merge to become one peak at higher temperature due to the effects of acceptor activation, dissociation of bound exciton from donors, and temperature-induced bandgap change. The 3.234 eV peak and weak peak at 3.162 eV at 14 K are separated from the FA emission peak by 71 meV and 143 meV, respectively. These energies can be associated with the phonon energy of ZnO (~72 meV), and therefore, these emissions are designated as the first and second phonon replicas of FA (FA-1LO and FA-2LO).[36] The observation of phonon replica indicates high optical quality of these nanowires.[37] Structural and optical characterizations of as grown nanowires in the reference sample (without DBR) can be found in the supplementary material (Figure S2), showing similar properties as these nanowires grown on DBR.

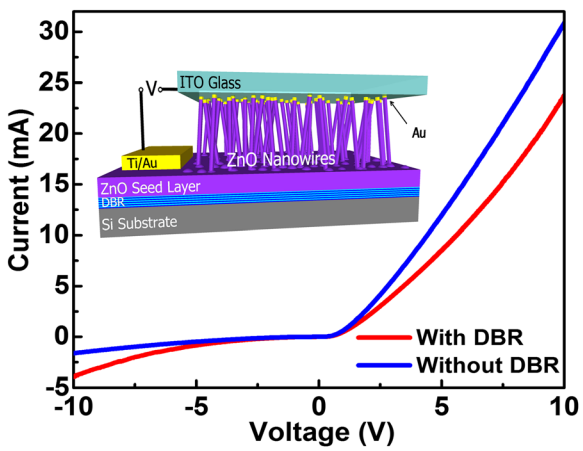

FIG. 2. I–V characteristics of Au-ZnO nanowire Schottky devices with and without DBR. Inset show Au-ZnO nanowire Schottky device schematics with DBR.

Figure 2 shows I–V characteristics of the random laser device with and without DBR. A schematic of the device with DBR is shown in the inset. A clear rectifying behavior is observed with a turn-on voltage of around 0.96 V from the device with DBR. Due to the large difference between work function of Au (~5.1 eV) and electron affinity of ZnO (~4.2 eV), a Schottky barrier is formed at the junction.[38] Since the Au/Ti metal on ZnO thin film is Ohmic,[16] the rectifying I–V together with a turn-on voltage, which is comparable with the Schottky barrier height suggest the formation of Au-ZnO nanowire Schottky junction.[39] The I–V characteristic of the reference sample (device without DBR) shows similar rectifying behavior and a turn-on voltage of ~1 V.

Figure 3(a) shows room temperature EL spectra of the laser device with DBR at different injection currents under forward bias which is designated as positive voltages on the Au contact. At lower injection currents, for example, 12 mA and 22 mA, weak spontaneous near band edge emission can be observed in the range of around 370–400 nm. As the current increases to 34 mA, a few low-intensity randomly distributed peaks start to appear on top of the spontaneous emission band. Beyond 34 mA, the emission peaks rapidly become stronger and sharper. At an injection current of 55 mA, many lasing peaks can be seen with a linewidth of around 0.23 nm and the EL intensity is greatly enhanced. The output power and integrated EL intensity (inset) as a function of injection current is shown in Figure 3(b), with which, a threshold current of ~37.7 mA can be estimated. EL spectra of the reference sample are shown in Figure 3(c). Similar to the EL spectra of the device with DBR shown in Figure 3(a), at relatively lower injection currents, only spontaneous emissions are observed while at higher injection currents, random lasing modes with unstable peak positions and mode separations are evident. These emissions originate from excitonic process, in which under forward bias limited excess holes are leaked from Au/ZnO junction to form excitons with incoming electrons from Au/Ti/ZnO film contact, and subsequently these excitons recombine to emit light.[29] Figure 3(d) shows output power and integrated EL intensity (inset) as a function of injection current of the reference sample. Clear lasing threshold behavior is observed and the threshold current is determined to be 68 mA, which is about 1.8 times higher than that of the device with DBR. The measured output powers at a wavelength of the strongest lasing mode near 385 nm are 123 nW and 30 nW at the same injection current of 75 mA for the devices with and without

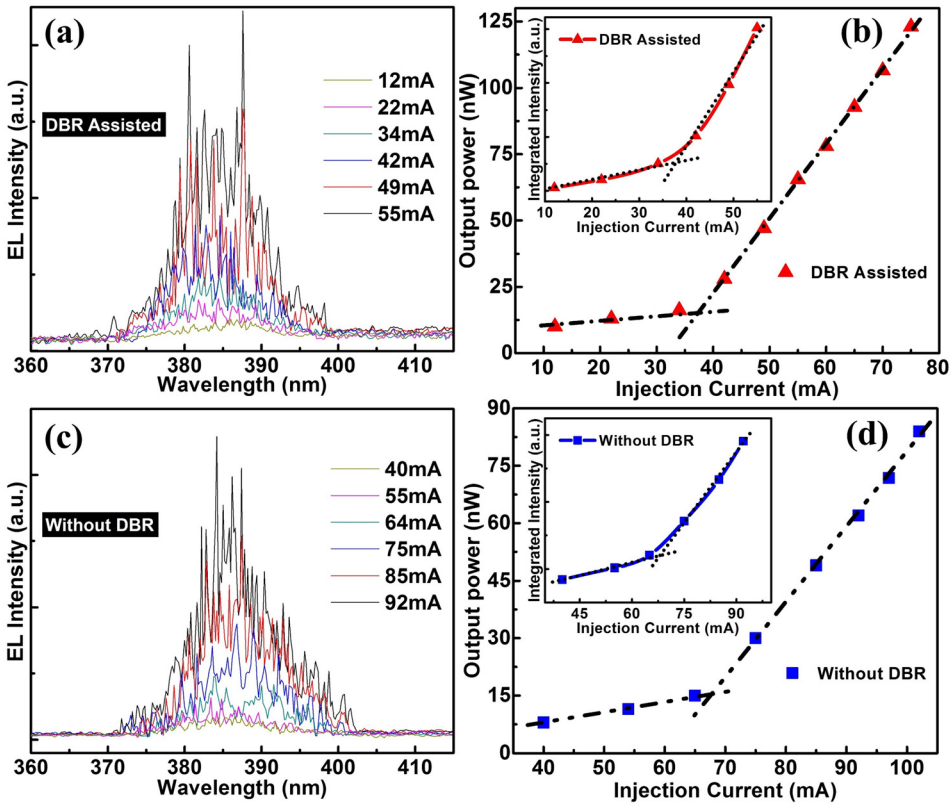

FIG. 3. (a) EL spectra of Au-ZnO nanowire Schottky device with DBR under different injection currents. (b) Output power and integrated intensities (inset) as functions of injection currents of DBR-assisted device, (c) EL spectra of Au-ZnO nanowire Schottky device without DBR under different injection currents, and (d) output power and integrated intensities (inset) as functions of injection currents of the Schottky device without DBR.

DBRs, respectively. Therefore, the output power is increased by almost 4 times when DBR is included.

Optical microscopic images of emission of both devices operated at the same current of 75 mA are shown in Figures 4(a) and 4(b), respectively. Blue-violet luminescence from the DBR-assisted device is brighter than that of the reference sample without DBR. Lasing phenomena of the devices with and without DBRs under an injection current of 75 mA and 100 mA, respectively, were also video-taped and have been uploaded as supporting data. Representative still images obtained from the videos of these laser devices with and without DBR are shown in Figure 4(c) (Multimedia view) and Figure 4(d) (Multimedia view), respectively. As observed from these videos, light comes out at random spots

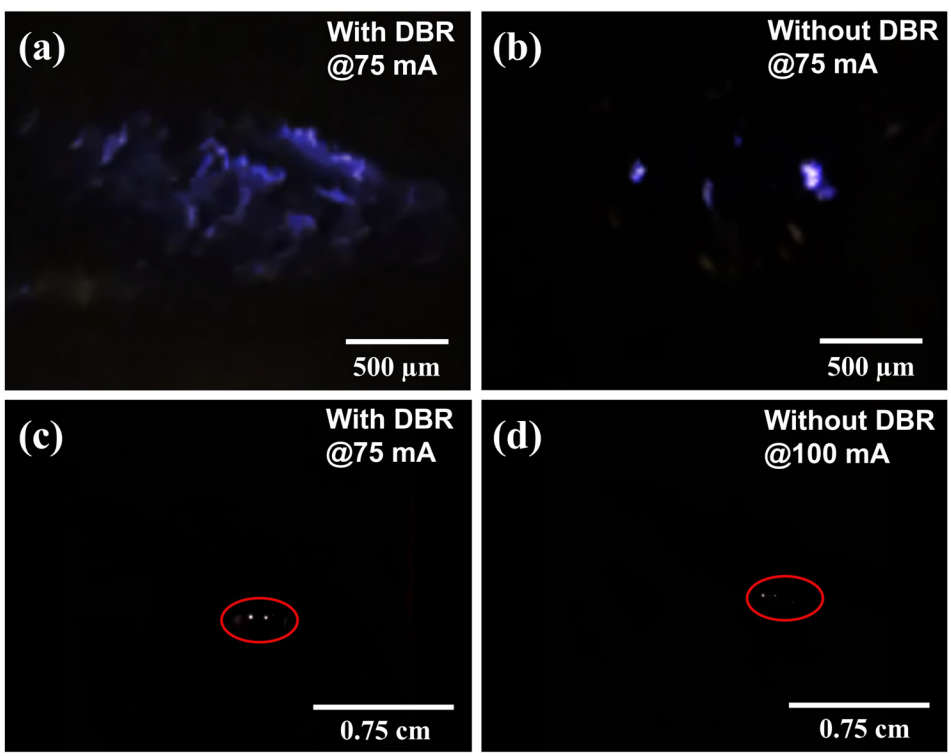

FIG. 4. Optical microscopy images of emission from laser devices (a) with DBR and (b) without DBR, both measured at 75 mA. Still images from the random laser video (c) with DBR measured at 75 mA [URL: http://dx.doi.org/10.1063/1.4967177.1] and (d) without DBR measured at 100 mA. (Multimedia view) [URL: http://dx.doi.org/10.1063/1.4967177.2]

from the surface of the devices as the time lapses. This result, clearly demonstrates that various random cavity loops are formed with time unpredictably, and in turn, the light spots are not spatially fixed. More frequent occurrence of brighter emission spots from the device with DBR even at a lower injection current than the reference sample indicates that the DBR-assisted Au/ZnO nanowire random laser has much stronger output, which is consistent with the EL spectra and power measurement results. This is because more light will be reflected back to the random nanowire medium with the presence of the DBR, leading to easier formation of random lasing cavities, in turn, higher output power.

In conclusion, DBR-assisted Au-ZnO nanowire Schottky junction random laser is fabricated and characterized. I–V characteristic of the device shows typical Schottky diode electrical property with a turn-on voltage of 0.96 V. Room temperature EL and output power characterizations, together with optical microscopy emission images and emission videos, demonstrate high-performance random lasing behavior as a result of excitonic recombination. Compared with a device without DBR, highly reflective DBR structure helps reduce the threshold current by 1.8 times and increase the output power by 4 times at the same injection current.

See supplementary material for the structural and optical properties of ZnO seed layer on bare Si (100) substrate.

This work was supported by SHINES, an Energy Frontier Research Center funded by the U.S. Department of Energy, Office of Science, Basic Energy Sciences under Award No. SC0012670.

[1]D. S. Wiersma, Nat. Phys. **4**, 359 (2008).
[2]B. Redding, M. A. Choma, and H. Cao, Nat. Photonics **6**, 355 (2012).
[3]Q. Song, S. Xiao, Z. Xu, V. M. Shalaev, and Y. L. Kim, Opt. Lett. **35**, 2624 (2010).
[4]Q. Song, Z. Xu, S. H. Choi, X. Sun, S. Xiao, O. Akkus, and Y. L. Kim, Biomed. Opt. Express **1**(5), 1401 (2010).
[5]D. S. Wiersma and S. Cavalieri, Nature **414**, 708 (2001).
[6]R. C. Polson and Z. V. Varden, Appl. Phys. Lett. **85**, 1289 (2004).
[7]D. M. Bagnall, Y. F. Chen, Z. Zhu, T. Yao, S. Koyama, M. Y. Shen, and T. Goto, Appl. Phys. Lett. **70**, 2230 (1997).
[8]N. M. Lawandy, R. M. Balachandran, A. S. L. Gomes, and E. Sauvain, Nature **368**, 436 (1994).
[9]H. Cao, Y. G. Zhao, H. C. Ong, S. T. Ho, J. Y. Dai, J. Y. Wu, and R. P. Chang, Appl. Phys. Lett. **73**, 3656 (1998).
[10]H. Cao, Y. G. Zhao, S. T. Ho, E. W. Seelig, Q. H. Wang, and R. P. Chang, Phys. Rev. Lett. **82**, 2278 (1999).
[11]H. Zhou, M. Wissinger, J. Fallert, R. Hauschild, F. Stelzl, C. Klingshirn, and H. Kalt, Appl. Phys. Lett. **91**, 181112 (2007).
[12]S. F. Yu, S. P. Lau, W. I. Park, and G. C. Yi, Appl. Phys. Lett. **84**, 3241 (2004).
[13]H. C. Hsu, C. Y. Wu, and W. F. Hsieh, J. Appl. Phys. **97**, 064315 (2005).
[14]S. F. Yu, C. Yuen, S. P. Lau, and H. W. Lee, Appl. Phys. Lett. **84**, 3244 (2004).
[15]C. Yuen, S. F. Yu, E. S. Leong, H. Y. Yang, S. P. Lau, N. S. Chen, and H. H. Hng, Appl. Phys. Lett. **86**, 31112 (2005).
[16]S. Chu, M. Olmedo, Z. Yang, J. Kong, and J. Liu, Appl. Phys. Lett. **93**, 181106 (2008).
[17]J. Kong, S. Chu, Z. Zuo, J. Ren, M. Olmedo, and J. Liu, Appl. Phys. A **107**, 971 (2012).
[18]Y. R. Ryu, J. A. Lubguban, T. S. Lee, H. W. White, T. S. Jeong, C. J. Youn, and B. J. Kim, Appl. Phys. Lett. **90**, 131115 (2007).
[19]H. K. Liang, S. F. Yu, and H. Y. Yang, Appl. Phys. Lett. **96**, 101116 (2010).
[20]E. S. P. Leong and S. F. Yu, Adv. Mater. **18**, 1685 (2006).
[21]S. B. Bashar, M. Suja, M. Morshed, F. Gao, and J. Liu, Nanotechnology **27**, 065204 (2016).
[22]J. Huang, S. Chu, J. Y. Kong, L. Zhang, C. M. Schwarz, G. P. Wang, L. Chernyak, Z. H. Chen, and J. L. Liu, Adv. Opt. Mater. **1**, 179 (2013).
[23]J. Huang, M. M. Morshed, Z. Zuo, and J. Liu, Appl. Phys. Lett. **104**, 131107 (2014).
[24]F. Schuster, B. Laumer, R. R. Zamani, C. Magén, J. R. Morante, J. Arbiol, and M. Stutzmann, ACS Nano **8**, 4376 (2014).
[25]Y. J. Lu, C. X. Shan, M. M. Jiang, G. C. Hu, N. Zhang, S. P. Wang, B. H. Li, and D. Z. Shen, Cryst. Eng. Commun. **17**, 3917 (2015).
[26]C. Y. Liu, H. Y. Xu, J. G. Ma, X. H. Li, X. T. Zhang, Y. C. Liu, and R. Mu, Appl. Phys. Lett. **99**, 063115 (2011).
[27]X. Ma, J. Pan, P. Chen, D. Li, H. Zhang, Y. Yang, and D. Yang, Opt. Express **17**, 14426 (2009).
[28]X. Y. Liu, C. X. Shan, S. P. Wang, Z. Z. Zhang, and D. Z. Shen, Nanoscale **4**, 2843 (2012).
[29]F. Gao, M. M. Morshed, S. B. Bashar, Y. D. Zheng, Y. Shi, and J. Liu, Nanoscale **7**, 9505 (2015).
[30]D. C. Look and B. Claflin, Phys. Status Solidi B **241**, 624 (2004).
[31]J. Xiao, Y. Wu, X. Bai, W. Zhang, and L. Yu, J. Phys. D: Appl. Phys. **41**, 135409 (2008).
[32]H. Cao, Opt. Photonics News **16**, 24 (2005).
[33]C. X. Shan, Z. Liu, and S. K. Hark, Appl. Phys. Lett. **92**, 073103 (2008).
[34]D. C. Look, B. Claflin, Y. I. Alivov, and S. J. Park, Phys. Status Solidi A **201**, 2203 (2004).
[35]J. E. Stehr, W. M. Chen, N. K. Reddy, C. W. Tu, and I. A. Buyanova, Sci. Rep. **5**, 13406 (2015).
[36]J. Dai, H. Liu, W. Fang, L. Wang, Y. Pu, Y. Chen, and F. Jiang, J. Cryst. Growth **283**, 93 (2005).
[37]B. K. Meyer, H. Alves, D. M. Hofmann, W. Kriegseis, D. Forster, F. Bertram, J. Christen, A. Hoffmann, M. Straßburg, M. Dworzak, U. Haboeck, and A. V. Rodina, Phys. Status Solidi B **241**, 231 (2004).
[38]L. J. Brillson and Y. Lu, J. Appl. Phys. **109**, 121301 (2011).
[39]Ş. Aydoğan, K. Çınar, H. Asıl, C. Coşkun, and A. Türüt, J. Alloys Compd. **476**, 913 (2009).